THE JOURNAL OF PHYSICAL CHEMISTRY B

ARTICLE

pubs.acs.org/JPCB

Unique Structural and Electronic Features of Perferryl−Oxo Oxidant in Cytochrome P450

Hiroshi Isobe,*,† Syusuke Yamanaka,† Mitsutaka Okumura,† Kizashi Yamaguchi,† and Jiro Shimada‡

†Department of Chemistry, Graduate School of Science, Osaka University, Toyonaka, Osaka 560-0043, Japan

‡Green Innovation Research Laboratories, NEC Corporation, 34, Miyukigaoka, Tsukuba, Ibaraki 305-8501, Japan

Supporting Information

ABSTRACT:

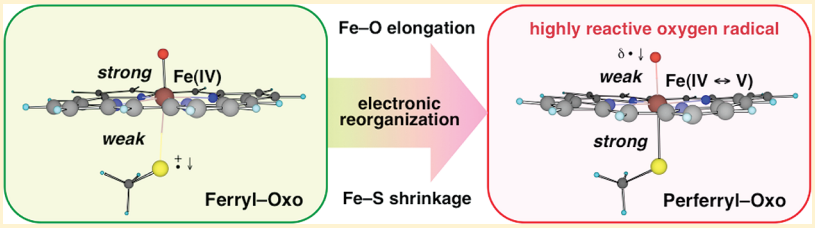

We have performed hybrid density functional theory (DFT) calculations on the geometric and electronic structures of low-lying doublet and quartet ferryl−oxo [Fe(IV)═O] oxidants and a doublet perferryl−oxo [Fe(V)═O] oxidant in Cytochrome P450. Fully optimized structures of compound I models have been determined, and the proper symmetry of wave functions has been restored by the spin-projection technique. The results show that the perferryl−oxo species is relatively low lying, as compared with the excited state of the ferryl−oxo species, if the iron−oxo bond is properly described as the mixing of several appropriate excited electronic configurations to minimize electron repulsion. This means that the perferryl−oxo species is virtually in a mixed-valent resonance state, ↑Fe(V)═O ↔ ↑Fe(IV)•↑−↓•O, containing a highly reactive pπ atomic oxygen radical. The anionic thiolate ligand acts as a Lewis σ base and functions to achieve the stability of the perferryl−oxo complex and to activate the oxo ligand trans to it by asymmetric bond distortion along the O−Fe−S axis by lengthening the Fe−O bond and shortening the Fe−S bond, prior to the hydrogen-atom abstraction from the substrate.

1. INTRODUCTION

Cytochrome P450 (P450) refers to an important and widely distributed class of heme-based monoxygenases and plays key roles in the biosynthesis of endogenous compounds such as cholesterol, steroids, and lipids; the detoxification of xenobiotics such as environmental pollutants; and drug metabolism in living organisms.[1] P450 enzymes employ an iron atom as its catalytic agent, which is coordinated by four nitrogen atoms of a protoporphyrin IX macrocycle and a cysteinate residue as the proximal ligand.[1] In most cases, P450 enzymes use molecular oxygen (O_2), two protons, and two electrons from NADH or NADPH to catalyze the oxidation of a wide variety of hydrophobic compounds, which include hydroxylation, epoxidation, *N*- and *O*-dealkylations, sulfoxidation, dehydrogenation, and so on.[1]

Due to their vital biological roles and medical implications, a considerable amount of experimental and theoretical investigations has been directed toward understanding of fundamental processes in the catalytic cycle of P450.[1,2] Although the details of the mechanism are not yet fully settled, it is generally accepted that, after the displacement of a distal water ligand in the ferric resting state of the enzyme by a substrate, the reductive activation of O_2 is achieved through several well-characterized states:[1−3] one-electron reduction of the ferric heme [Fe(III)]; reversible dioxygen binding to the reduced ferrous heme iron [Fe(II)] to form a ferrous−dioxygen [Fe(II)−OO] or ferric−superoxide [Fe(III)−OO^-] adduct; a second one-electron reduction to give a ferric−peroxide [Fe(III)−OO^{2-}] species, which can be protonated to produce a ferric−hydroperoxide [Fe(III)−OOH^-] complex, the so-called compound 0; and a second protonation followed by the release of a water molecule to generate a high-valent ferryl−oxo [Fe(IV)═O] complex with a porphyrin π-cation radical, known also as compound I (**1**, Chart 1), which is two-oxidation equivalents above the ferric resting state. This high-valent iron−oxo species **1** has generally been assumed to be the primary oxidant responsible for the energy-demanding two-electron oxidations of substrates.[4,5]

Very recently, Rittle and Green unambiguously characterized compound I as a ferryl−oxo unit antiferromagnetically coupled with a ligand-based radical in the stopped-flow reaction of *meta*-chloroperoxybenzoic acid with thermophilic P450 from *Sulfolobus acidocaldarious* by EPR, UV−visible, and Mössbauer spectroscopies.[5] Moreover, high-yield preparation of compound

Received: March 21, 2011
Revised: July 31, 2011
Published: August 03, 2011

Chart 1

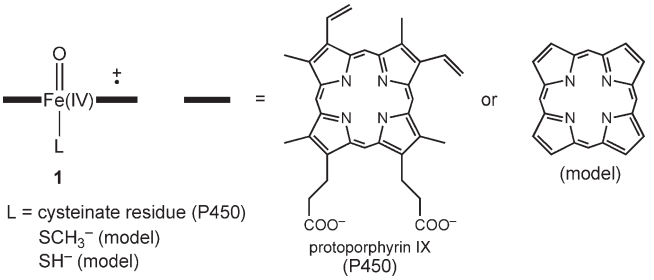

I (∼ 75%) enabled them to investigate its reactivity in oxidizing unactivated C−H bonds of lauric acid and to analyze kinetic isotope effects for the reaction.[5] By contrast, numerous attempts to detect compound I during the native catalytic cycle of P450, in which oxygen and redox equivalents are provided from O_2 and NAD(P)H via iron−sulfur protein or FAD/FMN-containing flavoprotein, have been unsuccessful.[1,6] This suggests that the actual oxidizing species is too reactive to be trapped under normal catalytic turnover conditions, probably due to a low barrier for C−H or C═C bond activation by compound I relative to that for the conversion of compound 0 to compound I.[2c] In the past, there have been arguments as to whether the excited states may have some impact on the reactivity of compound I. Isolobal analogy might allow us to draw parallels between the reactivities of $^{1,3}O_2$ and the ferryl ^{1,3}Fe(IV)═O unit,[7,8] while the involvement of the perferryl−oxo [Fe(V)═O] species was invoked to explain experimental results by laser flash photolysis (LFP),[9] although an objection was raised about the identity of the LFP-generated species.[10] Chen et al. performed extensive CASPT2/MM calculations for compound I of P450 and chloroperoxidase and indicated that compound I has more than 20 states jammed within 30 kcal mol^{-1}, of which the pentaradicaloid and perferryl states of relatively low energies (≤10 kcal mol^{-1}) may contribute the reactivity of compound I.[11] In this study, we have addressed the geometric and electronic structures of the several low-lying excited states of compound I, which include all doublet and quartet ferryl−oxo states of triradical character and a doublet perferryl−oxo state, by hybrid density functional theory (DFT) (B3LYP) calculations[12] followed by spin projection.[7a,13,14] It will be shown that the perferryl−oxo species is indeed low lying. Implications from fully optimized structures and spin-projected wave functions will be discussed to uncover the unique structural and electronic features of the perferryl−oxo oxidant.

2. COMPUTATIONAL DETAILS AND THEORETICAL BACKGROUNDS

2.1. Compound I Models. Compound I was modeled by an iron−oxo porphyrin complex with the side chains of the heme truncated. The proximal ligand was represented by either a methylthiolate anion (SCH_3^-) or a thiolate anion (SH^-), which we call the SCH_3 and SH models throughout this paper; the subscript SH (e.g., $\mathbf{1}_{SH}$) is used for the latter to distinguish the two models.

2.2. Methods. All geometry optimizations were performed using the unrestricted (U) B3LYP method[12] with an effective core potential basis set of double-ζ quality (CEP-31G),[15] hereafter denoted as BS1, implemented in Gaussian 03.[16] The level shifting method was used during the self-consistent field (SCF) procedure to improve convergence. Frequency calculations were performed with the same basis set to verify the nature of all stationary points and to derive zero-point vibrational corrections (ZPC) without scaling and thermodynamics effects at 298.15 K by statistical mechanics calculations. The final energetics was further evaluated by single-point calculations with an extensive all-electron basis set augmented with polarization and diffuse functions on all atoms, i.e., the Wachters (augmented with Bauschlicher f functions) basis set[17] on the Fe atom and the 6-31++G(d,p) basis set[18] on the C, H, O, N, and S atoms, labeled as BS2. Bulk polarity effect was evaluated by the CPCM-UAKS model[19] at the B3LYP/BS2 level. The dielectric constants (ε) of 2.247 and 36.64 were employed to represent benzene and acetonitrile environments.

2.3. Natural Orbital Analysis. To make a theoretical interpretation of the electronic characteristics of compound I, symmetry-adapted natural orbitals (ϕ) were determined by diagonalizing the spin-traced first-order density matrices [$\rho(\mathbf{r}',\mathbf{r})$] of broken-symmetry (BS) solutions (canonical Kohn−Sham orbitals, $\psi^{\alpha,\beta}$, or corresponding orbitals, $\psi^{\pm}$),[20] as given by eq 1, in which N^+ and N^- are the numbers of up and down spins satisfying the inequality, $N^+ \geq N^-$.

$$\begin{aligned}\rho(\mathbf{r}',\mathbf{r}) &= \sum_{i=1}^{N^+} \psi_i^{\alpha}(\mathbf{r}')\psi_i^{\alpha *}(\mathbf{r}) + \sum_{i=1}^{N^-} \psi_i^{\beta}(\mathbf{r}')\psi_i^{\beta *}(\mathbf{r}) \\ &= \sum_{i=1}^{N^-} [n_i\phi_i(\mathbf{r}')\phi_i^{*}(\mathbf{r}) + n_{-i}\phi_{-i}(\mathbf{r}')\phi_{-i}^{*}(\mathbf{r})] \\ &\quad + \sum_{i=1}^{N^+ - N^-} \phi_{0,i}(\mathbf{r}')\phi_{0,i}^{*}(\mathbf{r}) \end{aligned} \quad (1)$$

The natural orbitals (ϕ) can be transformed into the corresponding orbitals ($\psi^{\pm}$),[21] as shown in eq 2, in which ω_i is the orbital mixing angle($0 \leq \omega_i \leq \pi/2$).

$$\psi_i^{\pm}(\mathbf{r}) = \cos\omega_i\phi_i(\mathbf{r}) \pm \sin\omega_i\phi_{-i}(\mathbf{r}) \quad (2a)$$

$$\psi_{0,i}^{+}(\mathbf{r}) = \phi_{0,i}(\mathbf{r}) \quad (2b)$$

The eigenvalues, $n_{\pm i}$ and 1, can be interpreted as the occupation numbers of natural orbitals, $\phi_{\pm i}$ and $\phi_{0,i}$, and used to extract important orbitals that characterize the electronic property of the system under consideration. In a doublet triradical system such as compound I ($N^+ - N^- = 1$), there should be three natural orbitals with an occupation number close to 1.0, which are responsible for static correlation effects. One of them arises from eq 2b and has an exactly single occupancy, which we call below SONO (ϕ_{SONO}), while the other two originate from eq 2a and make a pair with fractional occupation numbers, $1 \pm \langle\psi_{HONO}^{+}|\psi_{HONO}^{-}\rangle$, which we call HONO and LUNO (ϕ_{HONO} and ϕ_{LUNO}). The orbital overlap integral between the corresponding orbitals $\psi_{HONO}^{\pm}$ (T), which is related with the occupation number of HONO by eq 3, can be chosen as a measure of the extent of bonding interaction between formally paired electrons in $\psi_{HONO}^{\pm}$.

$$T \equiv \langle\psi_{HONO}^{+}|\psi_{HONO}^{-}\rangle = \cos 2\omega_{HONO} = n_{HONO} - 1 \quad (3)$$

We evaluated the effective bond order of the iron−oxo core (b_{FeO}) from the sum of the occupation numbers of natural orbitals to consider pseudo excitation from the bonding orbital

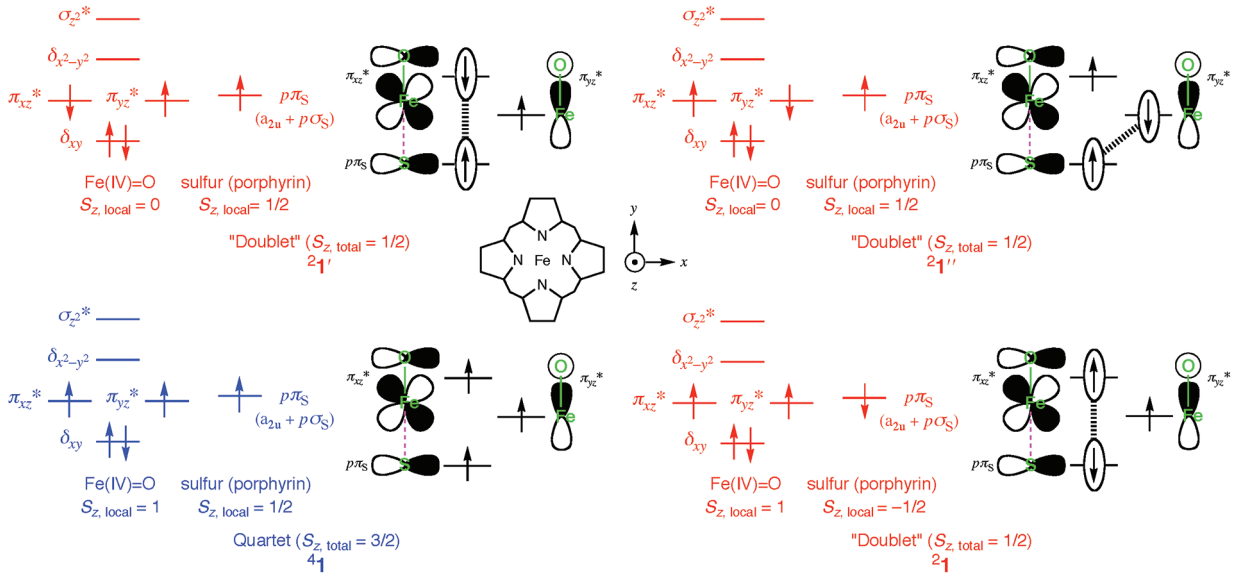

Figure 1. Electronic configurations of ferryl compound I (**1**); electrons in formally paired spin-polarized orbitals, $\psi^{\pm}_{\mathrm{HONO}}$ (eq 2a), are marked by two ellipses with a hashed line representing a bonding interaction between the two spin-paired electrons in $\psi^{\pm}_{\mathrm{HONO}}$.

Table 1. Relative Energies, Bond Lengths, Bond Stretching Frequencies, and Mulliken Spin Densities of Several Configurations of Compound I (1) at the B3LYP/BS2//BS1 Level

		ΔE + ZPC[a]		bond length[b]		frequency[c]		Mulliken spin density[d]			
model	species	BS1	BS2	r_{FeO}	r_{FeS}	ν_{FeO}	ν_{FeS}	Fe	O	SCH_3 or SH	porphyrin
$L = SCH_3^-$	$^4\mathbf{1}$	0.0	0.0	1.646	2.682	890.5	116.5	1.07 (1.16)	0.94 (0.88)	0.77 (0.79)	0.22 (0.18)
	$^2\mathbf{1}$	−0.1 (−0.2)	−0.2 (−0.3)	1.646	2.688	895.6	114.0	1.19 (1.24)	0.91 (0.86)	−0.80 (−0.82)	−0.31 (−0.28)
	$^2\mathbf{1}'$	8.8 (13.3)	9.0 (13.1)	1.662	2.630	607.7	116.6	−0.45 (−0.19)	0.39 (0.16)	0.76 (0.78)	0.30 (0.25)
	$^2\mathbf{1}''$	9.3 (14.0)	8.8 (13.6)	1.646	2.688	883.0	115.4	0.00 (−0.02)	−0.04 (−0.02)	0.79 (0.81)	0.26 (0.23)
	$^2\mathbf{1}^*$	11.3 (−)	12.6 (−)	1.777	2.339	525.6	310.8	1.66 (1.41)	−0.85 (−0.78)	0.36 (0.49)	−0.16 (−0.12)
$L = SH^-$	$^4\mathbf{1}_{\mathrm{SH}}$	0.0	0.0	1.652	2.615	873.5	146.4	1.04 (1.13)	0.97 (0.90)	0.56 (0.59)	0.44 (0.38)
	$^2\mathbf{1}_{\mathrm{SH}}$	0.0 (−0.1)	−0.2 (−0.3)	1.650	2.631	884.1	145.9	1.21 (1.26)	0.91 (0.86)	−0.61 (−0.63)	−0.52 (−0.48)
	$^2\mathbf{1}'_{\mathrm{SH}}$	8.5 (12.6)	9.4 (13.5)	1.694	2.550	500.8	162.4	−0.70 (−0.46)	0.62 (0.42)	0.52 (0.55)	0.56 (0.49)
	$^2\mathbf{1}^*_{\mathrm{SH}}$	8.8 (−)	13.5 (−)	1.782	2.352	566.7	302.7	1.90 (1.81)	−0.84 (−0.80)	0.14 (0.12)	−0.20 (−0.13)

[a] Relative energies including ZPC with respect to the $^4\mathbf{1}$ (or $^4\mathbf{1}_{\mathrm{SH}}$) configuration are given in kcal mol^{-1}; values with AP correction using eq 5 are given in parentheses. [b] Fe−O (r_{FeO}) and Fe−S (r_{FeS}) bond lengths are given in angstroms. [c] Unscaled stretching frequencies of Fe−O (ν_{FeO}) and Fe−S (ν_{FeS}) bonds are given in cm^{-1}. [d] Values with BS1 (BS2) are given out of (in) parentheses.

(contributing to a positive bond order, $n_\kappa/2$) to the antibonding one (contributing to a negative bond order, $-n_{\kappa^*}/2$),[22] as shown in eq 4.

$$b_{\mathrm{FeO}} \equiv \sum_{\kappa=\sigma_{z^2},\pi_{xz},\pi_{yz}} (n_\kappa - n_{\kappa^*})/2 \qquad (4)$$

All active orbitals (HONO, LUNO, and SONO) and their occupation numbers, as well as Mulliken charge and spin populations, for structures reported in this paper are available as Supporting Information.

3. RESULTS AND DISCUSSION

3.1. Electronic Structures of Ferryl−Oxo Species. Figure 1 indicates the occupancies of the high-lying occupied and low-lying unoccupied orbitals of compound I, **1**, which are composed of metal-based five d-type orbitals (δ_{xy}, π_{xz}^*, π_{yz}^*, $\delta_{x^2-y^2}$, and $\sigma_{z^2}^*$), of which two orthogonal π_{xz}^* and π_{yz}^* orbitals and the $\sigma_{z^2}^*$ orbital are the out-of-phase combinations of the 3d orbitals of the Fe atom (d_{xz}, d_{yz}, and d_{z^2}) with the 2p orbitals of the O atom (p_x, p_y, and p_z) in π and σ fashions, and one ligand-based orbital, which is either a porphyrin a_{2u} orbital (in D_{4h} symmetry) mixed with a sulfur $p\sigma_S$ orbital or a sulfur $p\pi_S$ orbital, depending on the ligand representation.[2] The ground and several low-lying states of **1** are usually considered to involve three or five unpaired electrons placed in the above six orbitals.[2,11,23] If we restrict the orbital assignment of the five electrons only to covalent configurations of triradical character, in which the two Fe−O π^* orbitals and the ligand-based orbital (χ_L) are singly occupied, $(\delta_{xy})^2(\pi_{xz}^*)^1(\pi_{yz}^*)^1(\chi_L)^1$ (χ_L = a_{2u} or π_S), there are four different situations possible with respect to the spins of these electrons, $^4\mathbf{1}$, $^2\mathbf{1}$, $^2\mathbf{1}'$, and $^2\mathbf{1}''$, as shown in Figure 1. Among these, three configurations, $^2\mathbf{1}$, $^2\mathbf{1}'$, and $^2\mathbf{1}''$, are not eigenstates of the $\hat{S}^2$ operator; the proper linear combinations of them should lead to two independent doublet states ($S_{z,\mathrm{total}}$ = 1/2) and one quartet state ($S_{z,\mathrm{total}}$ = 1/2), as described later. The quartet state

dx.doi.org/10.1021/jp206004y |J. Phys. Chem. B 2011, 115, 10730–10738

with $S_{z,\mathrm{total}} = 1/2$ should be energetically degenerate with the high-spin component ($S_{z,\mathrm{total}} = 3/2$) of the quartet state ($^4\mathbf{1}$) in the absence of a magnetic field.

We have characterized the four electronic configurations, $^4\mathbf{1}$, $^2\mathbf{1}$, $^2\mathbf{1}'$, and $^2\mathbf{1}''$, by DFT calculations for the SCH_3 and SH models of compound I, as summarized in Table 1. The Mulliken population analysis serves to identify the $^4\mathbf{1}$ and $^2\mathbf{1}$ configurations, since these two configurations have a characteristic "local triplet" ($\uparrow\uparrow$, $S_{z,\mathrm{local}} = 1$)[24] electron-pair situation at the ferryl−oxo core with the only difference being the relative orientation of an electron spin residing in the ligands ($S_{z,\mathrm{local}} = 1/2$ or $-1/2$). In $^4\mathbf{1}$, the three unpaired electrons are all aligned with up spin, $(\delta_{xy})^2(\pi_{xz}^*)^\uparrow(\pi_{yz}^*)^\uparrow(\chi_L)^\uparrow$, while in $^2\mathbf{1}$, the unpaired electron on the ligands points in an opposite direction, $(\delta_{xy})^2(\pi_{xz}^*)^\uparrow(\pi_{yz}^*)^\uparrow(\chi_L)^\downarrow$. The computed spin density distributions of $^4\mathbf{1}$ and $^2\mathbf{1}$ are indeed as we expect from the orbital occupancies; net spin population on the FeO moiety for $^4\mathbf{1}$ ($^2\mathbf{1}$) is close to 2, and that on the ligands is almost unity with positive (negative) sign, as shown in Table 1. Changing the modeling of the proximal ligand from SCH_3^- to SH^- is reflected in the spin distribution on the ligands for the ground-state configurations. The SCH_3 model causes the porphyrin-based radical, which resides in the combined porphyrin a_{2u} and sulfur $p\sigma_S$ orbital, to rise above the sulfur-based radical, which is mostly contracted on the sulfur $p\pi_S$ orbital, while in the SH model, the porphyrin-based radical is placed below the sulfur-based radical, in accordance with previous calculations.[25,26] Such a spin density shift from the sulfur to the porphyrin ring is responsible for relatively high Fe−S bond stretching frequencies for the SH model (ν_{FeS} = 146.4 and 145.9 cm^{-1} for $^4\mathbf{1}_{SH}$ and $^2\mathbf{1}_{SH}$), as compared with those for the SCH_3 model (116.5 and 114.0 cm^{-1} for $^4\mathbf{1}$ and $^2\mathbf{1}$).

Unlike the $^4\mathbf{1}$ and $^2\mathbf{1}$ cases, it is not straightforward to discriminate between the $^2\mathbf{1}'$ and $^2\mathbf{1}''$ configurations from information on spin density distribution only, since both configurations have a common "local singlet" ($\uparrow\downarrow$, $S_{z,\mathrm{local}} = 0$)[24] spin array at the ferryl−oxo core with an up-spin density on the ligand ($S_{z,\mathrm{local}} = 1/2$), $(\delta_{xy})^2(\pi_{xz}^*)^\downarrow(\pi_{yz}^*)^\uparrow(\chi_L)^\uparrow$ and $(\delta_{xy})^2(\pi_{xz}^*)^\uparrow(\pi_{yz}^*)^\downarrow(\chi_L)^\uparrow$. As far as the SCH_3 model is concerned, it will be convenient to use the natural orbital analysis to define the $^2\mathbf{1}'$ and $^2\mathbf{1}''$ configurations. Degenerate e_{xz} and e_{yz} orbitals for the iron−oxo porphyrin complex void of the SCH_3 ligand belong to the a′ and a″ representations of the C_S subgroup of the C_{4v} point group. HONO and LUNO for $^2\mathbf{1}'$ and $^2\mathbf{1}''$ are combined to describe a weak bonding interaction between electrons in the $p\pi_S$ orbital of the thiolate ligand and in either the π_{xz}^* or π_{yz}^* orbital of the ferryl-oxo core. Inspection of the phase patterns of HONO and LUNO, therefore, enables us to distinguish between $^2\mathbf{1}'$ and $^2\mathbf{1}''$ by determining whether the constituent $p\pi_S$ orbital lies in the same plane containing the constituent π_{xz}^* orbital or in the nodal plane of the π_{yz}^* orbital; we define the former case as the $^2\mathbf{1}'$ configuration and the latter as $^2\mathbf{1}''$. As a result, the SONO, which accommodates a formally noninteracting electron, should be the π_{yz}^* orbital in $^2\mathbf{1}'$ and the π_{xz}^* orbital in $^2\mathbf{1}''$. Figure 1 also schematically shows the bonding patterns beside the corresponding orbital diagrams; electrons in formally paired spin-polarized orbitals, $\psi_{\mathrm{HONO}}^{\pm}$ (eq 2a), are marked by two ellipses with a hashed line representing a bonding interaction between the two spin-paired electrons in $\psi_{\mathrm{HONO}}^{\pm}$. One might expect that, in both $^2\mathbf{1}'$ and $^2\mathbf{1}''$, there should be no net spin density on the FeO moiety, since the π_{xz}^* and π_{yz}^* orbitals occupied by up- and down-spin electrons may be delocalized over the Fe and O atoms. As for $^2\mathbf{1}''$, this is indeed the case, as shown in Table 1; however, up- and down-spin densities appear in $^2\mathbf{1}'$ as Fe↓(−0.45)−O↑(0.39) (BS1) and Fe↓(−0.19)−O↑(0.16) (BS2) (Table 1). The reason for this can be traced to the presence of a third unpaired electron in the thiolate ligand. Although the overlap interaction between the π_{yz}^* and $p\pi_S$ orbitals is very small in $^2\mathbf{1}''$ ($T = \langle\pi_{yz}^*|\pi_S\rangle$ = 0.02), nonnegligible overlap between the π_{xz}^* orbital and the appropriately orientated $p\pi_S$ orbital in $^2\mathbf{1}'$ ($T = \langle\pi_{xz}^*|\pi_S\rangle$ = 0.13) can accumulate more electron density in the region between the Fe and S atoms. As a result, in $^2\mathbf{1}'$, a down-spin electron in the π_{xz}^* orbital and an up-spin electron in the SONO (π_{yz}^*) tend to distribute themselves toward the Fe and O centers so that their repulsive interaction is minimized. This spin polarization is accompanied at the expense of decreasing π bonding in $^2\mathbf{1}'$, which is manifested in a smaller Fe−O bond stretching frequency (ν_{FeO} = 607.7 cm^{-1}) than that in $^2\mathbf{1}''$ (883.0 cm^{-1}), and this is also responsible for small differences in energy and geometry between $^2\mathbf{1}'$ and $^2\mathbf{1}''$, which would vanish if there really were no interaction between the iron−oxo core and the ligand. Concerning the SH model, we can no longer discriminate between the $^2\mathbf{1}'_{SH}$ and $^2\mathbf{1}''_{SH}$ configurations, unless the $p\sigma_S$ orbital is mixed with the $p\pi_S$ orbital to generate a tilted hybrid orbital on the sulfur. B3LYP calculations converged to only the lower configuration, which may be identified as $^2\mathbf{1}'_{SH}$ by the overlap between the π-like hybrid orbital on the S atom and the suitably oriented π_{xz}^* orbital with T = 0.17. The symmetry breaking and the lack of equivalence between two BS solutions are inherent in the SCF procedure using average effective electrostatic field.

The energies of the four electronic configurations, $^4\mathbf{1}$, $^2\mathbf{1}$, $^2\mathbf{1}'$, and $^2\mathbf{1}''$, show the pairwise degeneracy, as shown in Table 1. A large energy splitting of "local triplet" $[(\pi_{xz}^*)^\uparrow(\pi_{yz}^*)^\uparrow$ for $^4\mathbf{1}$ and $^2\mathbf{1}]$ and "local singlet" $[(\pi_{xz}^*)^\downarrow(\pi_{yz}^*)^\uparrow$ and $(\pi_{xz}^*)^\uparrow(\pi_{yz}^*)^\downarrow$ for $^2\mathbf{1}'$, and $^2\mathbf{1}'']$ electron-pair situations at the ferryl−oxo core (ca. 9 kcal mol^{-1}) is caused by significant electron−electron repulsion, while weak interaction between the ferryl−oxo core and the ligand ($T < 0.2$) is reflected in almost degenerate ground and excited configurations within a range of 0.5 kcal mol^{-1}. However, BS solutions obtained from the B3LYP method are usually not spin-adapted states, and therefore, several resonance structures of symmetry breaking are required to represent an appropriate wave function for a real state. For example, two states of the FeO^{2+} moiety can be described as in-phase and out-of-phase resonance states between two degenerate configurations, $(\pi_{xz}^*)^\downarrow(\pi_{yz}^*)^\uparrow \leftrightarrow (\pi_{xz}^*)^\uparrow(\pi_{yz}^*)^\downarrow$, which are isoelectronic with the $^3\Sigma_g^-$ and $^1\Delta_g$ states of O_2.[7,8] One approach to restore the proper symmetry of wave functions from several BS solutions in the mean field approximation is the resonating broken-symmetry configuration iteration (RBS-CI).[27] The problems of BS solutions can also be treated through the application of the approximate spin projection (AP) scheme.[7a,14] Here, let us make use of the AP procedure to estimate the energy differences between the ground and excited doublet states of the ferryl−oxo species for the SCH_3 model. In this scheme, we simply assume that the doublet BS wave function, which is composed of a single Slater determinant with $S_z = 1/2$, is a linear combination of two doublet states with $S_z = 1/2$ and the $S_z = 1/2$ component of a quartet state and that the quartet BS wave function with $S_z = 3/2$ does not involve any significant amount of spin contamination from higher spin states.[14a] On these assumptions, it is possible to write out an appropriate correction term for the elimination of the component of the quartet state. The total projected energy for the doublet state, $^2E_{AP}$, is given by eq 5, in which $^XE_{BS}$ and $^X\langle\hat{S}^2\rangle_{BS}$ stand for the total energy and the expectation value of

the spin operator $\hat{S}^2$ taken with respect to the BS wave function for the spin multiplicity X.

$$ {}^2E_{AP} = {}^2E_{BS} + \frac{{}^2\langle\hat{S}^2\rangle_{BS} - 0.75}{{}^4\langle\hat{S}^2\rangle_{BS} - {}^2\langle\hat{S}^2\rangle_{BS}} ({}^2E_{BS} - {}^4E_{BS}) \quad (5) $$

Approximately spin-projected $^2\mathbf{1}'$ and $^2\mathbf{1}''$, represented by AP-$^2\mathbf{1}'$ and AP-$^2\mathbf{1}''$, are estimated to lie 13.5 (13.4) and 14.2 (13.9) kcal mol^{-1} above approximately spin-projected $^2\mathbf{1}$, denoted by AP-$^2\mathbf{1}$, with BS1 (BS2). These energy gaps are considerably small, as compared with the $^3\Sigma_g^-$ and $^1\Delta_g$ energy separation for O_2 [22.6 kcal mol^{-1} (experiment),[28] 21.4 kcal mol^{-1} (AP-B3LYP/6-31+G*)[29]].

We can understand what causes the overstabilizations of AP-$^2\mathbf{1}'$ and AP-$^2\mathbf{1}''$ relative to the ground state by looking at exact spin-projected wave functions, $|\text{P-}^2\mathbf{1}'\rangle$ and $|\text{P-}^2\mathbf{1}''\rangle$, corresponding to spin-projected $^2\mathbf{1}'$ and $^2\mathbf{1}''$, as shown in eqs 6 and 7, which can be generated by operating with the spin-projection operator, $\hat{O} = (\hat{S}^2 - 15\hbar^2/4)/(-3\hbar^2)$,[13] on BS wave functions for the three-electron system, $|\overline{\pi}_{xz}^*\pi_{yz}^*\pi_S\rangle$ and $|\pi_{xz}^*\overline{\pi}_{yz}^*\pi_S\rangle$ (N is a normalizing factor); note that π_{xz}^*, π_{yz}^*, and π_S should be read as corresponding orbitals.

$$ N\hat{O}|\overline{\pi}_{xz}^*\pi_{yz}^*\pi_S\rangle = 6^{-1/2}[|(\overline{\pi}_{xz}^*\pi_{yz}^* - \pi_{xz}^*\overline{\pi}_{yz}^*)\pi_S\rangle - |\pi_{yz}^*(\overline{\pi}_{xz}^*\pi_S - \pi_{xz}^*\overline{\pi}_S)\rangle] \equiv |\text{P-}^2\mathbf{1}'\rangle \quad (6) $$

$$ N\hat{O}|\pi_{xz}^*\overline{\pi}_{yz}^*\pi_S\rangle = 6^{-1/2}[|(\pi_{xz}^*\overline{\pi}_{yz}^* - \overline{\pi}_{xz}^*\pi_{yz}^*)\pi_S\rangle + |\pi_{xz}^*(\overline{\pi}_{yz}^*\pi_S - \pi_{yz}^*\overline{\pi}_S)\rangle] \equiv |\text{P-}^2\mathbf{1}''\rangle \quad (7) $$

These spin-projected wave functions for $^2\mathbf{1}'$ and $^2\mathbf{1}''$ are not orthogonal to each other. In fact, three wave functions, $|\text{P-}^2\mathbf{1}'\rangle$, $|\text{P-}^2\mathbf{1}''\rangle$, and $|\text{P-}^2\mathbf{1}\rangle$ ($\equiv N\hat{O}|\pi_{xz}^*\pi_{yz}^*\overline{\pi}_S\rangle$), make an "angle" of 120° with each other, in the sense that $\langle\text{P-}^2\mathbf{1}'|\text{P-}^2\mathbf{1}''\rangle = \langle\text{P-}^2\mathbf{1}''|\text{P-}^2\mathbf{1}\rangle = \langle\text{P-}^2\mathbf{1}|\text{P-}^2\mathbf{1}'\rangle = \cos 120°$; i.e., these wave functions are linearly dependent. Each spin-projected wave function in eqs 6 and 7 can be decomposed into two terms. The first term represents two singly occupied π_{xz}^* and π_{yz}^* orbitals coupled to generate a local singlet pair at the ferryl−oxo core with an isolated unpaired electron at the ligand, and by analogy with the $^1\Delta_g$ state of O_2, strongly destabilizes these doublet states relative to the ground state due to electron repulsion. On the other hand, the second term describes a π-bonding interaction between the ferryl−oxo core and the SCH_3 ligand, which offsets a part of the energy increase due to the first term and leads to a total energy gap that is substantially smaller than that between $^1O_2$ and $^3O_2$.

It will be more satisfactory and instructive to examine how the above two wave functions in eqs 6 and 7 transform by adding and subtracting them, as shown in eqs 8 and 9.

$$ |{}^2\mathbf{1}' \leftrightarrow {}^2\mathbf{1}''\rangle_S \equiv 3^{-1/2}[|\text{P-}^2\mathbf{1}'\rangle - |\text{P-}^2\mathbf{1}''\rangle] = 2^{-1/2}|(\overline{\pi}_{xz}^*\pi_{yz}^* - \pi_{xz}^*\overline{\pi}_{yz}^*)\pi_S\rangle \quad (8) $$

$$ \begin{aligned} |{}^2\mathbf{1}' \leftrightarrow {}^2\mathbf{1}''\rangle_T &\equiv -[|\text{P-}^2\mathbf{1}'\rangle + |\text{P-}^2\mathbf{1}''\rangle] \\ &= 6^{-1/2}[|\pi_{yz}^*(\overline{\pi}_{xz}^*\pi_S - \pi_{xz}^*\overline{\pi}_S)\rangle \\ &\quad -|\pi_{xz}^*(\overline{\pi}_{yz}^*\pi_S - \pi_{yz}^*\overline{\pi}_S)\rangle] \\ &= 6^{-1/2}[2|\pi_{xz}^*\pi_{yz}^*\overline{\pi}_S\rangle - |(\overline{\pi}_{xz}^*\pi_{yz}^* + \pi_{xz}^*\overline{\pi}_{yz}^*)\pi_S\rangle] \\ &= N\hat{O}|\pi_{xz}^*\pi_{yz}^*\overline{\pi}_S\rangle \end{aligned} \quad (9) $$

This linear transformation resolves the near degeneracy of the two nonorthogonal wave functions, $|\text{P-}^2\mathbf{1}'\rangle$ and $|\text{P-}^2\mathbf{1}''\rangle$, by lowering their in-phase combination and raising their out-of-phase combination, and gives rise to a new set of wave functions, $|{}^2\mathbf{1}' \leftrightarrow {}^2\mathbf{1}''\rangle_S$ and $|{}^2\mathbf{1}' \leftrightarrow {}^2\mathbf{1}''\rangle_T$, that forms a linearly independent orthogonal set. Not only does the mixing remove all the ligand−heme interaction from one of the two linear combinations, but it also eliminates local spin contamination at the ferryl−oxo moiety from the two doublet wave functions. The out-of-phase combination, $|{}^2\mathbf{1}' \leftrightarrow {}^2\mathbf{1}''\rangle_S$, is characterized by a pure local singlet state of the ferryl−oxo core with an isolated unpaired electron at the ligand, as shown in eq 8. The ligand−heme interaction is squeezed into the in-phase combination, $|{}^2\mathbf{1}' \leftrightarrow {}^2\mathbf{1}''\rangle_T$, as indicated in the second line of eq 9, which can also be interpreted as the superposition of the $S_z = 1$ and $S_z = 0$ components of the local triplet state of the ferryl−oxo core via an intervening unpaired electron on the ligand, as shown in the third line of eq 9. This orthogonal set of wave functions, $|{}^2\mathbf{1}' \leftrightarrow {}^2\mathbf{1}''\rangle_S$ and $|{}^2\mathbf{1}' \leftrightarrow {}^2\mathbf{1}''\rangle_T$, therefore, has a perfect isoelectronic analogy to the $^1\Delta$ and $^3\Sigma$ wave functions for O_2 and Fe(IV)=O ion and is much more convenient to analyze the electronic structures of compound I than the set employed before. In this paper, these locally symmetry-adapted states are symbolized by the subscripts, S and T.

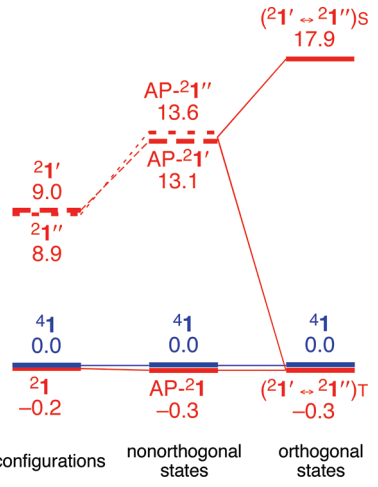

Figure 2. Relative energies of various ferryl−oxo configurations ($^2\mathbf{1}$, $^2\mathbf{1}'$, and $^2\mathbf{1}''$) and states [AP-$^2\mathbf{1}$, AP-$^2\mathbf{1}'$, AP-$^2\mathbf{1}''$, $(^2\mathbf{1}' \leftrightarrow {}^2\mathbf{1}'')_S$, and $(^2\mathbf{1}' \leftrightarrow {}^2\mathbf{1}'')_T$ (= AP-$^2\mathbf{1}$)] of compound I (SCH_3 model, **1**) at the B3LYP/BS2//BS1 level; relative energies with reference to the $^4\mathbf{1}$ configuration (state) are given in kcal mol^{-1}.

Since we have already used the AP scheme to obtain approximate values for the energy differences between the ground and excited doublet states in the nonorthogonal form, let us use these results to approximately assess the energy gap between two orthogonal components for the doublet state, $|{}^2\mathbf{1}' \leftrightarrow {}^2\mathbf{1}''\rangle_S$ and $|{}^2\mathbf{1}' \leftrightarrow {}^2\mathbf{1}''\rangle_T$. From eqs 8 and 9, we can write the total energy for $|{}^2\mathbf{1}' \leftrightarrow {}^2\mathbf{1}''\rangle_S$, as given by eq 10, since $|{}^2\mathbf{1}' \leftrightarrow {}^2\mathbf{1}''\rangle_T = N\hat{O}|\pi_{xz}^*\pi_{yz}^*\overline{\pi}_S\rangle$.

$$ \begin{aligned} {}^2E({}^2\mathbf{1}' \leftrightarrow {}^2\mathbf{1}'')_S &= (2/3)[{}^2E(\text{P-}{}^2\mathbf{1}') + {}^2E(\text{P-}{}^2\mathbf{1}'')] - {}^2E({}^2\mathbf{1}' \leftrightarrow {}^2\mathbf{1}'')_T/3 = (2/3)[{}^2E(\text{P-}{}^2\mathbf{1}') \\ &\quad + {}^2E(\text{P-}{}^2\mathbf{1}'')] - {}^2E(\text{P-}{}^2\mathbf{1})/3 \sim (2/3)[{}^2E_{AP}({}^2\mathbf{1}') \\ &\quad + {}^2E_{AP}({}^2\mathbf{1}'')] - {}^2E_{AP}({}^2\mathbf{1})/3 \end{aligned} \quad (10) $$

The final results are summarized in Figure 2; note that the effect of symmetry breaking on the geometry is small (Table 1) and thus is neglected in the estimation. The out-of phase resonance state of ferryl compound I [$(^2\mathbf{1}' \leftrightarrow {}^2\mathbf{1}'')_S$] analogous

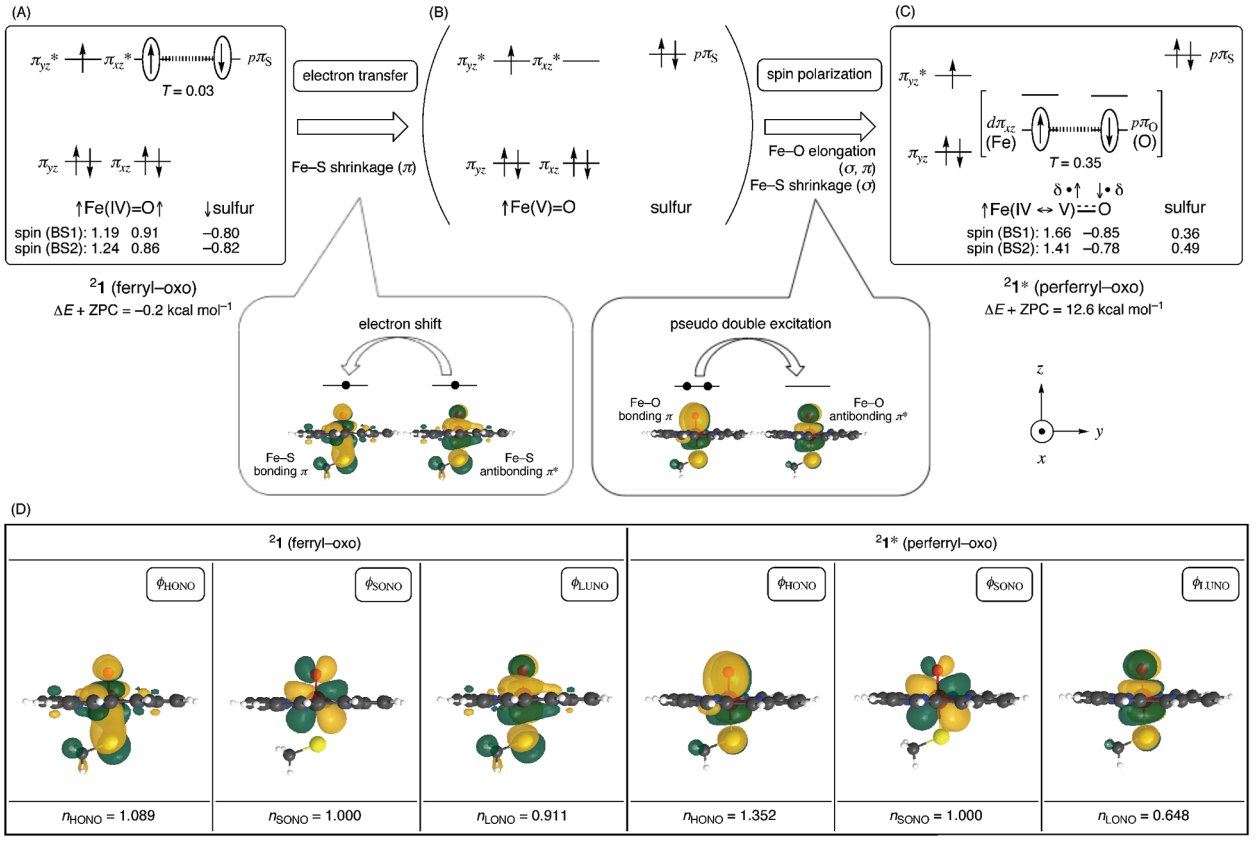

Figure 3. Molecular orbital explanation of the electronic reorganization from the ferryl−oxo (A) to perferryl−oxo (B,C) species. (D) HONO (ϕ_{HONO}), LUNO (ϕ_{LUNO}), and SONO (ϕ_{SONO}) and their occupation numbers (n_{HONO}, n_{LUNO}, and n_{SONO}) for the ferryl−oxo ($^2\mathbf{1}$) and perferryl−oxo ($^2\mathbf{1}^*$) species at the B3LYP/BS1 level.

to the $^1\Delta_g$ state of O_2 is now estimated to lie about 18.4 (18.2) kcal mol^{-1} above the ground state $[(^2\mathbf{1}' \leftrightarrow {}^2\mathbf{1}'')_T]$ analogous to the $^3\Sigma_g^-$ state of O_2 with BS1 (BS2), which agrees fairly well with the CASPT2/MM results (SH model, 18.3−18.4 kcal mol^{-1}).[11] It follows that, within the validity of the AP scheme, the $(^2\mathbf{1}' \leftrightarrow {}^2\mathbf{1}'')_S$ state has too high energy that the thermal excitation to this state will be inhibited in the onset of the hydrogen-atom abstraction from the C−H bond of the substrate by compound I, which is the initial step for alkane hydroxylation in the oxygen rebound mechanism.[30] Even if the energy gap between $(^2\mathbf{1}' \leftrightarrow {}^2\mathbf{1}'')_S$ and $(^2\mathbf{1}' \leftrightarrow {}^2\mathbf{1}'')_T$ shrinks during the reaction and hence $(^2\mathbf{1}' \leftrightarrow {}^2\mathbf{1}'')_S$ becomes accessible, the analogy between O_2 and the Fe(IV)═O moiety does not necessarily apply to the reactivity of compound I. In fact, at the maximum 50% of any one state is a mixture of the other state, since any superposed states, $\sin\theta|^2\mathbf{1}' \leftrightarrow {}^2\mathbf{1}''\rangle_T + \cos\theta|^2\mathbf{1}' \leftrightarrow {}^2\mathbf{1}''\rangle_S$ and $\cos\theta|^2\mathbf{1}' \leftrightarrow {}^2\mathbf{1}''\rangle_T - \sin\theta|^2\mathbf{1}' \leftrightarrow {}^2\mathbf{1}''\rangle_S$, are also doublet states of triradical character.

3.2. Electronic Structures of Perferryl−Oxo Species. According to the oxidation number rules, the orbital occupancy of the perferryl−oxo [Fe(V)═O] species, $^2\mathbf{1}^*$, can be formally described as $(\delta_{xy})^2(\pi_{xz}^*)^0(\pi_{yz}^*)^1(\chi_L)^2$; hereafter, we denote the perferryl species with the asterisk symbol (*). The electronic conversion from the tetravalent ferryl−oxo species $^2\mathbf{1}$ to the pentavalent perferryl−oxo one $^2\mathbf{1}^*$ requires formally the transition of one electron from the π_{xz}^* orbital of the ferryl−oxo core to the χ_L (π_S or a_{2u}) orbital in the ligands, as indicated in Figure 3 (A → B) for the SCH_3 model ($\chi_L = \pi_S$); accordingly, the formal Fe−O bond order increases from 2.0 to 2.5. In preceding B3LYP studies, the perferryl−oxo species was predicted to lie much higher in energy than the ferryl−oxo one by 16−22 kcal mol^{-1} (B3LYP)[26b] and by 46 kcal mol^{-1} (TDDFT/MM),[31] while the Fe(IV)−Fe(V) energy gap was estimated to be considerably small (≤10 kcal mol^{-1}) at the CASPT2/MM level.[11]

We have also examined this species by full optimizations with the B3LYP method. Calculations make it clear that π electrons in the Fe(V)═O core are actually highly prone to spin polarization, i.e., partial separation of up- and down-spin electrons in the bonding π orbital into spatially different regions, since electrons paired in the orbital repel each other electrostatically. Restricted open-shell B3LYP calculations indeed show instability relative to BS solutions, in which π electrons now occupy two different orbitals as a result of the mixing of the vacant π_{xz}^* orbital into the π_{xz} orbital with in- and out-of-phase combinations for up and down spins, as shown in Figure 3 (B → C). It is instructive to compare the natural orbitals for the doublet ferryl−oxo species $^2\mathbf{1}$ with those for the doublet perferryl−oxo species $^2\mathbf{1}^*$, as displayed in Figure 3D. Both species have the same π_{yz}^* orbital of the iron−oxo core as SONO. The HONO and LUNO of $^2\mathbf{1}$ have a large coefficient in the sulfur $p\pi_S$ orbital, as compared with those of $^2\mathbf{1}^*$. The decrease in the relative weight of the $p\pi_S$ orbital on going from $^2\mathbf{1}$ to $^2\mathbf{1}^*$ indicates the annihilation of a radical hole on the ligand. Another important difference between $^2\mathbf{1}$ and $^2\mathbf{1}^*$ is found at the amplitude pattern of HONO along the O−Fe−S axis, which has out-of-phase overlapping between the $d\pi_{xz}$ and $p\pi_O$ atomic orbitals on Fe and O in $^2\mathbf{1}$, but in $^2\mathbf{1}^*$ no such sign inversion, instead acquiring a node between Fe and S. The

absence of a nodal plane through the Fe−O bond in the HONO of ^{2}**1***, together with fractional occupancies of the HONO and LUNO ($\pi_{xz} \rightarrow \pi_{xz}^*$ pseudo double excitation), causes spin polarization within the iron−oxo core, rather than spread over the thiolate ligand as in the case of ^{2}**1**. The fully delocalized π_{xz} orbital of the iron−oxo core is now deformed into partially localized in-plane $d\pi_{xz}$ and $p\pi_O$ orbitals on the Fe and O atoms, thereby giving rise to a partial breaking of the π bond and a specific net spin density, which arise from a contribution from the resonance structures, $^{\uparrow}$Fe(V)═O ↔ $^{\uparrow}$Fe(IV)•$^{\uparrow}$−$^{\downarrow}$•O. The actual oxidation state should be somewhere between Fe(IV) with complete spin polarization and Fe(V) with no spin polarization. Such a mixed-valent resonance state for ^{2}**1*** can be validated by the fact that the mixing of $|\pi_{xz}\overline{\pi}_{xz}\pi_{yz}^*\rangle$ and its doubly excited configuration $|\pi_{xz}^*\overline{\pi}_{xz}^*\pi_{yz}^*\rangle$ is caused by a significant exchange integral of the electron repulsion operator between the orbitals that span the same sets of atoms, $\langle\pi_{xz}\overline{\pi}_{xz}\pi_{yz}^*|\hat{H}|\pi_{xz}^*\overline{\pi}_{xz}^*\pi_{yz}^*\rangle = [\pi_{xz}\pi_{xz}^*|\pi_{xz}\pi_{xz}^*] \gg 0$. In fact, the weights of the $|\pi_{xz}\overline{\pi}_{xz}\pi_{yz}^*\rangle$ and $|\pi_{xz}^*\overline{\pi}_{xz}^*\pi_{yz}^*\rangle$ configurations in ^{2}**1***, which can be evaluated from the unnormalized spin-projected wave function for the three-electron system, denoted by $|\text{P-}^2\mathbf{1}^*\rangle$, as shown in eq 11 (note that π_{xz}, π_{xz}^*, and π_{yz}^* should be read as natural orbitals), are calculated to be 64.6 (65.0) and 14.8 (13.9) % with BS1 (BS2).

$$
\begin{aligned}
|\text{P-}^2\mathbf{1}^*\rangle &= 3\cos^2\omega_{\text{HONO}}|\pi_{xz}\overline{\pi}_{xz}\pi_{yz}^*\rangle \\
&- 3\sin^2\omega_{\text{HONO}}|\pi_{xz}^*\overline{\pi}_{xz}^*\pi_{yz}^*\rangle \\
&- \sqrt{6}\cos\omega_{\text{HONO}}\sin\omega_{\text{HONO}}\{6^{-1/2}[2|\pi_{xz}\overline{\pi}_{yz}^*\pi_{xz}^*\rangle \\
&- |\overline{\pi}_{xz}\pi_{yz}^*\pi_{xz}^*\rangle - |\pi_{xz}\pi_{yz}^*\overline{\pi}_{xz}^*\rangle]\} \qquad (11)
\end{aligned}
$$

The effective bond order for the perferryl−oxo bond (eq 4), which is not only associated with formal bond formation but also with the correlation of electrons via two-electron exchange integral, is now considerably less (1.9 with both BS1 and BS2), as compared with the formal bond order of 2.5 with electrons pairing in the delocalized π_{xz} orbital. The localization of π electrons on individual atomic centers causes a rise of spin density on iron from 1.19 (1.24) in ^{2}**1** to 1.66 (1.41) in ^{2}**1*** with BS1 (BS2) and an appearance of negative spin density on the oxo ligand [−0.85 (−0.78)], as shown in Figure 3C. This $p\pi_O$ atomic oxygen radical is expected to have a high reactivity toward the hydrogen abstraction from an inert C−H bond, as is the case in hydroxyl radical.[32] In fact, additional calculations show that ^{2}**1*** can abstract a hydrogen atom from propane with an activation barrier of only 2.5 (2.0) kcal mol^{-1} with BS1 (BS2).

The electronic reorganization from ^{2}**1** to ^{2}**1*** leaves distinct signatures not only on the spin density distribution but also on the equilibrium bond lengths and bond stretching frequencies for the O−Fe−S unit, as shown in Table 1: a long length (r_{FeO} = 1.777 Å) and a low frequency (ν_{FeO} = 525.6 cm^{-1}) of the Fe−O bond and a short length (r_{FeS} = 2.339 Å) and a high frequency (ν_{FeS} = 310.8 cm^{-1}) of the Fe−S bond for the perferryl−oxo species ^{2}**1***, as compared with those for the ferryl−oxo species ^{2}**1** (r_{FeO} = 1.646 Å, ν_{FeO} = 895.6 cm^{-1}, r_{FeS} = 2.688 Å, and ν_{FeS} = 114.0 cm^{-1}). These features provide important information about the extent of bonding for the Fe−O and Fe−S bonds; their strengths alternate by the electronic reorganization, leading to a weaker Fe−O bond and a stronger Fe−S bond for ^{2}**1*** than ^{2}**1**. This phenomenon can be accounted for by the fact that two ligands trans to each other use the same orbitals on the Fe ion for σ and π bonding. In the event that allows (forbids) the mixing of an unoccupied antibonding orbital with an occupied bonding one of different local symmetry, a relevant bond should elongate (shrink) so that the energy levels of these orbitals come closer to (separate more from) each other. Concerning the Fe−S bond, the electron shift (A → B in Figure 3) occurs from the antibonding Fe−S π orbital (corresponding to the LUNO of ^{2}**1**) to the bonding one (the HONO of ^{2}**1**), accompanied by a decrease in the Fe−S bond length, so that the π-bonding interaction between the thiolate ligand and the Fe atom strengthens due to incoming electron density between the Fe and S atoms. Spin polarization of π electrons in the Fe−S bond is almost entirely quenched. In contrast, the elongation of the Fe−O bond from short distances is required for inducing another spin polarization of π electrons within the iron−oxo core (B → C in Figure 3), which involves a pseudo excitation from the bonding Fe−O π orbital (corresponding to the HONO of ^{2}**1***) to the antibonding one (the LUNO of ^{2}**1***) and hence transfers electron density from the overlap region to the outside. This energetically costly process should be mitigated by the trans influence of the negatively charged thiolate ligand, which donates σ electrons, making the Fe−O bond weaker with concomitant Fe−S bond compression and Fe−O bond extension. This type of σ bonding of the thiolate ligand to a d-metal atom is sometimes referred to as the "push" effect. The net energy required for the electronic reorganization from ^{2}**1** to ^{2}**1*** in the mixed-valent state is now estimated to be 11.4 (12.8) kcal mol^{-1} with BS1 (BS2), which should be compared with the significant excitation energy from ^{2}**1** to $(^2\mathbf{1}' \leftrightarrow {}^2\mathbf{1}'')_S$ [18.3 (18.1) kcal mol^{-1}], in which case the π-bonding interaction between the iron−oxo core and the ligand is formally absent (eq 8).

The conversion of the quartet ferryl−oxo configuration ^{4}**1** to the quartet perferryl one ^{4}**1*** with the same orbital occupancy as that for ^{2}**1***, $(\delta_{xy})^2(d\pi_{xz})^{\uparrow}(p\pi_O)^{\uparrow}(\pi_{yz}^*)^{\uparrow}(p\pi_S)^2$, is forbidden at around the equilibrium Fe−O bonding distance of ^{2}**1*** ($r_{FeO} \sim$ 1.8 Å) by significant Pauli repulsion for a pair of electrons with parallel spin residing in the overlapping $d\pi_{xz}$ and $p\pi_O$ atomic orbitals in the same plane.[33] Although the AP scheme cannot be applied to the ^{2}**1*** configuration, the BS energy of ^{2}**1*** has a significance, in that it provides an upper bound to the energy of the spin-adapted mixed-valent state. If we assume that ^{4}**1*** lies more than 3 (6) kcal mol^{-1} above ^{2}**1*** and has a $^4\langle\hat{S}^2\rangle_{BS}$ value of about 3.8, the approximately spin-projected energy gap between ^{4}**1** and ^{2}**1*** is estimated to be less than 10 kcal mol^{-1} using eq 5 and $^2\langle\hat{S}^2\rangle_{BS}$ = 1.68 (1.66) with BS1 (BS2), which is in qualitative agreement with the CASPT2/MM results (SH model, ≤ 10 kcal mol^{-1}).[11]

We could also locate a doublet perferryl species for the SH model, denoted by ^{2}**1**$_{SH}$*. From Table 1, one can see that, like ^{2}**1***, ^{2}**1**$_{SH}$* has a longer and weaker Fe−O bond (r_{FeO} = 1.782 Å and ν_{FeO} = 566.7 cm^{-1}) and a shorter and stronger Fe−S bond (r_{FeS} = 2.352 Å and ν_{FeS} = 302.7 cm^{-1}), as compared with the ferryl−oxo species, ^{4}**1**$_{SH}$ and ^{2}**1**$_{SH}$ (r_{FeO} = 1.65 Å, r_{FeS} = 2.62−2.63 Å, ν_{FeO} = 874−884 cm^{-1}, and ν_{FeS} = 146 cm^{-1}). The electronic conversion from the ferryl to perferryl species should be attended by asymmetric bond distortion along the O−Fe−S axis by lengthening the Fe−O bond (by about 0.13 Å) and shortening the Fe−S bond (by about 0.27 Å) with the assistance of σ donation from the basic SH$^-$ ligand to the Fe center. The Fe−O bond order for ^{2}**1**$_{SH}$* so generated is 1.85, according to eq 4, indicating a partial cleavage of Fe−O π bond. As a result, a highly reactive atomic oxygen radical with a significant negative spin [−0.84 (−0.80) with BS1 (BS2)] is prepared to abstract a hydrogen atom from the substrate.

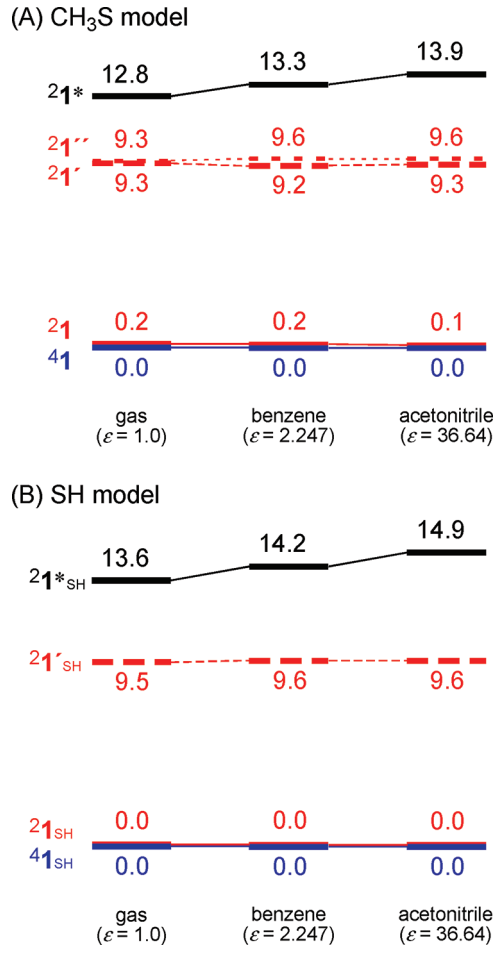

Figure 4. Influence of bulk polarity on the relative stabilities of the $^4\mathbf{1}$, $^2\mathbf{1}$, $^2\mathbf{1}'$, $^2\mathbf{1}''$, $^2\mathbf{1}^*$ configurations at the B3LYP/BS2//BS1 level by the CPCM-UAKS method; relative free energies with reference to the $^4\mathbf{1}$ configuration are given in kcal mol^{-1}.

3.3. Bulk Polarity Effect. The effect of solvent polarity on the relative stabilities of $^4\mathbf{1}$, $^2\mathbf{1}$, $^2\mathbf{1}'$, $^2\mathbf{1}''$, and $^2\mathbf{1}^*$ has been examined by the CPCM-UAKS method at the B3LYP/BS2 level for both the SCH_3 and SH models, as summarized in Figure 4. Incorporation of polarizing medium is found to raise the perferryl−oxo species $^2\mathbf{1}^*$ in free energy relative to the pair of the ground configurations ($^{2,4}\mathbf{1}$) by about 0.5−0.6 kcal mol^{-1} in benzene and 1.1−1.3 kcal mol^{-1} in acetonitrile, while exhibiting a very small effect on the relative free energies of the excited configurations for the ferryl−oxo species ($^2\mathbf{1}'$ and $^2\mathbf{1}''$) to within 0.3 kcal mol^{-1}.

4. CONCLUSIONS

We have performed hybrid DFT calculations on the geometric and electronic structures of low-lying doublet and quartet ferryl−oxo oxidants and a doublet perferryl−oxo oxidant as a new important low-lying active species for compound I models ($\mathbf{1}$, L = SCH_3^- or SH^-). There are notable structural differences in the O−Fe−S unit between the ferryl and perferryl species, depending on the mode of spin polarization. The ferryl−oxo species, $^4\mathbf{1}$, $^2\mathbf{1}$, $^2\mathbf{1}'$, and $^2\mathbf{1}''$, have a short and strong Fe−O π bond and a long and weak Fe−S π bond with an unpaired electron largely localized on the S atom (or the porphyrin ring), thereby leading to the pairwise degeneracy of the four configurations. The fact that the out-of-phase resonance state between the degenerate excited configurations, $(^2\mathbf{1}' \leftrightarrow {}^2\mathbf{1}'')_S$, which is isoelectronic with the $^1\Delta$ excited state for O_2 and FeO^{2+} ion, is as much as 18 kcal mol^{-1} higher than the ground state makes it a less plausible candidate for the active oxidant in P450. By contrast, the highly oxidized perferryl−oxo species, $^2\mathbf{1}^*$, has a short and strong Fe−S π bond and a long and weak Fe−O π bond with an unpaired electron effectively localized on the O atom. This unique bonding pattern of $^2\mathbf{1}^*$ as a mixed-valent resonance state, $\uparrow$Fe(V)═O ↔ $\uparrow$Fe(IV)•$\uparrow$−$\downarrow$•O, can be properly described only when the interaction between several appropriate excited configurations is included in the wave function to deal with spin polarization, as shown in eq 11. As compared with $(^2\mathbf{1}' \leftrightarrow {}^2\mathbf{1}'')_S$, $^2\mathbf{1}^*$ is relatively low lying with an adiabatic excitation energy of less than 12.6 (14.5) kcal mol^{-1} for the CH_3S (HS) model. The electron-rich SCH_3^- and SH^- ligands both serve to achieve the stability of the perferryl−oxo complex. This ability can be attributed to the presence of a lone pair on the sulfur atom as a Lewis σ base (electron-pair donor). One important consequence of this bonding is the effect on the strength of the Fe−O π bond. Strong σ donation to the iron atom results in a weakening of the Fe−O bond with a corresponding decrease in stretching frequency, thereby promoting spin polarization of π electrons within the iron−oxo core and hence the generation of a highly reactive pπ atomic oxygen radical. Thus, the appreciably basic thiolate ligand can also function to activate the oxo ligand trans to it, prior to the hydrogen-atom abstraction from the substrate. More details of the reactivity of the perferryl−oxo oxidant and its role in the native cycle will be discussed in a forthcoming publication.

■ ASSOCIATED CONTENT

Supporting Information. Three figures of natural orbitals and potential curves; one table of Mulliken charge and spin densities; and Cartesian coordinates, absolute energies, and $\langle \hat{S}^2 \rangle$ values of optimized structures reported. This material is available free of charge via the Internet at http://pubs.acs.org.

■ AUTHOR INFORMATION

Corresponding Author
*E-mail: isobe@chem.sci.osaka-u.ac.jp.

■ ACKNOWLEDGMENT

This study was performed through the "Development of Basic Technologies for Advanced Production Methods Using Microorganism Functions" project from the New Energy and Industrial Technology Development Organization (NEDO).

■ REFERENCES

(1) (a) Sono, M.; Roach, M. P.; Coulter, E. D.; Dawson, J. H. *Chem. Rev.* **1996**, *96*, 2841. (b) Guengerich, F. P. *Chem. Res. Toxicol.* **2001**, *14*, 611. (c) Meunier, B.; de Visser, S. P.; Shaik, S. *Chem. Rev.* **2004**, *104*, 3947. (d) Denisov, I. G.; Makris, T. M; Sligar, S. G.; Schlichting, I. *Chem. Rev.* **2005**, *105*, 2253. (e) Ortiz de Montellano, P. R. *Chem. Rev.* **2010**, *110*, 932. (f) Omura, T.; Ishimura, Y.; Fujii-Kuriyama, Y., Eds. *Cytochrome P-450*, 2nd ed.; Kodansha: Tokyo, 1993. (g) Ortiz de Montellano, P. R., Ed. *Cytochrome P450: Structure, Mechanism, and Biochemistry*, 3rd ed.; Kluwer Academic/Plenum Publishers: New York, 2005. (h) Sigel, A., Sigel, H., Sigel, R. K. O., Eds. *The Ubiquitous Role of Cytochrome P450 Proteins In Metal Ions in Life Sciences*; John Wiley & Sons Ltd: Chichester, England, 2007; Vol. 3.

(2) (a) Loew, G. H.; Harris, D. L. *Chem. Rev.* **2000**, *100*, 407. (b) Shaik, S.; Kumar, D.; de Visser, S. P.; Altun, A.; Thiel, W. *Chem. Rev.* **2005**, *105*, 2279. (c) Shaik, S.; Cohen, S.; Wang, Y.; Chen, H.; Kumar, D.; Thiel, W. *Chem. Rev.* **2010**, *110*, 949.

(3) (a) Schlichting, I.; Berendzen, J.; Chu, K.; Stock, A. M.; Maves, S. A.; Benson, D. E.; Sweet, R. M.; Ringe, D.; Petsko, G. A.; Sligar, S. G. *Science* **2000**, *287*, 1615. (b) Davydov, R.; Makris, T. M.; Kofman, V.; Werst, D. E.; Sligar, S. G.; Hoffman, B. M. *J. Am. Chem. Soc.* **2001**, *123*, 1403.

(4) (a) Egawa, T.; Shimada, H.; Ishimura, Y. *Biochem. Biophys. Res. Commun.* **1994**, *201*, 1464. (b) Kellner, D. G.; Hung, S.-C.; Weiss, K. E.; Sligar, S. G. *J. Biol. Chem.* **2002**, *277*, 9641. (c) Dowers, T. S.; Rock, D. A.; Rock, D. A.; Jones, J. P. *J. Am. Chem. Soc.* **2004**, *126*, 8868. (d) Spolitak, T.; Dawson, J. H.; Ballou, D. P. *J. Biol. Chem.* **2005**, *280*, 20300.

(5) Rittle, J.; Green, M. T. *Science* **2010**, *330*, 933.

(6) (a) Jung, C. *Biochim. Biophys. Acta* **2011**, *1814*, 46. (b) Jung, C.; de Vries, S.; Schünemann, V. *Arch. Biochem. Biophys.* **2011**, *507*, 44.

(7) (a) Yamaguchi, K.; Takahara, Y.; Fueno, T. In *Applied Quantum Chemistry*; Smith, V. H., Jr., Scheafer, H. F., III, Morokuma, K., Eds; D. Reidel: Boston, 1986; p155. (b) Shoji, M.; Isobe, H.; Saito, T.; Yabushita, H.; Koizumi, K.; Kitagawa, Y.; Yamanaka, S.; Kawakami, T.; Okumura, M.; Hagiwara, M.; Yamaguchi, K. *Int. J. Quantum Chem.* **2008**, *108*, 631. (c) Isobe, H.; Nishihara, S.; Shoji, M.; Yamanaka, S.; Shimada, J.; Hagiwara, M.; Yamaguchi, K. *Int. J. Quantum Chem.* **2008**, *108*, 2991. (d) Yamaguchi, K.; Shoji, M.; Isobe, H.; Yamanaka, S.; Shimada, J.; Kitagawa, K.; Okumura, M. *Polyhedron* **2009**, *28*, 2044.

(8) Shaik, S.; Filatov, M.; Schröder, D.; Schwartz, H. *Chem.—Eur. J.* **1998**, *4*, 193.

(9) (a) Newcomb, M.; Zhang, R.; Chandrasena, R. E.; Halgrimson, J. A.; Horner, J. H.; Makris, T. M.; Sligar, S. G. *J. Am. Chem. Soc.* **2006**, *128*, 4580. (b) Sheng, X.; Horner, J. H.; Newcomb, M. *J. Am. Chem. Soc.* **2008**, *130*, 13310. (c) Pan, Z.; Wang, Q.; Sheng, X.; Horner, J. H.; Newcomb, M. *J. Am. Chem. Soc.* **2009**, *131*, 2621. (d) Sheng, X.; Zhang, H.; Im, S.-C.; Horner, J. H.; Waskell, L.; Hollenberg, P. F.; Newcomb, M. *J. Am. Chem. Soc.* **2009**, *131*, 2971. (e) Wang, Q.; Sheng, X.; Horner, J. H.; Newcomb, M. *J. Am. Chem. Soc.* **2009**, *131*, 10629.

(10) Rittle, J.; Younker, J. M.; Green, M. T. *Inorg. Chem.* **2010**, *49*, 3610.

(11) Chen, H.; Song, J.; Lai, W.; Wu, W.; Shaik, S. *J. Chem. Theory Comput.* **2010**, *6*, 940.

(12) (a) Becke, A. D. *Phys. Rev. A* **1988**, *38*, 3098. (b) Lee, C.; Yang, W.; Parr, R. G. *Phys. Rev. B* **1988**, *37*, 785. (c) Becke, A. D. *J. Chem. Phys.* **1993**, *98*, 5648.

(13) Löwdin, P.-O. *Phys. Rev.* **1955**, *97*, 1509.

(14) (a) Yamaguchi, K.; Jensen, F.; Dorigo, A.; Houk, K. N. *Chem. Phys. Lett.* **1988**, *149*, 537. (b) Yamaguchi, K.; Takahara, Y.; Fueno, T.; Houk, K. N. *Theoret. Chem. Acta* **1988**, *73*, 337.

(15) (a) Stevens, W. J.; Basch, H.; Krauss, M. *J. Chem. Phys.* **1984**, *81*, 6026. (b) Stevens, W. J.; Krauss, M.; Basch, H.; Jasien, P. G. *Can. J. Chem.* **1992**, *70*, 612. (c) Cundari, T. R.; Stevens, W. J. *J. Chem. Phys.* **1993**, *98*, 5555.

(16) Frisch, M. J.; Trucks, G. W.; Schlegel, H. B.; Scuseria, G. E.; Robb, M. A.; Cheeseman, J. R.; Montgomery, Jr., J. A.; Vreven, T.; Kudin, K. N.; Burant, J. C.; et al. *Gaussian 03*, revision E.01; Gaussian, Inc.: Wallingford, CT, 2004.

(17) Wachters, A. J. H. *J. Chem. Phys.* **1970**, *52*, 1033. (b) Bauschlicher, C. W., Jr.; Langhoff, S. R.; Barnes, L. A. *J. Chem. Phys.* **1989**, *91*, 2399.

(18) Hehre, W. J.; Radom, L.; Schleyer, P. v. R.; Pople, J. A. *Ab Initio Molecular Orbital Theory*; Wiley: New York, 1986.

(19) (a) Klamt, A.; Schüürmann, G. *J. Chem. Soc., Perkin Trans. 2* **1993**, 799. (b) Andzelm, J; Kölmel, C.; Klamt, A. *J. Chem. Phys.* **1995**, *103*, 9312. (c) Barone, V.; Cossi, M. *J. Phys. Chem. A* **1998**, *102*, 1995. (d) Cossi, M.; Rega, N.; Scalmani, G.; Barone, V. *J. Comput. Chem.* **2003**, *24*, 669.

(20) Löwdin, P.-O. *Phys. Rev.* **1955**, *97*, 1474.

(21) Harriman, J. E. *J. Chem. Phys.* **1964**, *40*, 2827.

(22) (a) Nishino, M.; Yamanaka, S.; Yoshioka, Y.; Yamaguchi, K. *J. Phys. Chem. A* **1997**, *101*, 705. (b) Isobe, H.; Takano, Y; Kitagawa, Y; Kawakami, T; Yamanaka, S; Yamaguchi, K; Houk, K. N. *Mol. Phys.* **2002**, *100*, 717. (c) Isobe, H.; Takano, Y; Kitagawa, Y; Kawakami, T; Yamanaka, S; Yamaguchi, K; Houk, K. N. *J. Phys. Chem. A* **2003**, *107*, 682.

(23) Hirao, K.; Kumar, D.; Thiel, W.; Shaik, S. *J. Am. Chem. Soc.* **2005**, *127*, 13007.

(24) By using double quotation marks as "local singlet" and "local triplet", we mean that they are quasi-classical spin arrangement, not quantum mechanical resonance states as described in eqs 8 and 9. We have used the prime symbol (′) or the double prime symbol (″) to specify "local singlet" coupling between two electrons in the orthogonal π_{xz}^* and π_{yz}^* orbitals.

(25) Green, M. T. *J. Am. Chem. Soc.* **1999**, *121*, 7939.

(26) (a) Ogliaro, F.; Cohen, S.; Filatov, M.; Harris, N.; Shaik, S. *Angew. Chem., Int. Ed.* **2000**, *39*, 3851. (b) Ogliaro, F.; de Visser, S. P.; Groves, J. T.; Shaik, S. *Angew. Chem., Int. Ed.* **2001**, *40*, 2874.

(27) The resonating DFT CI method is currently under development. For the resonating Hartree−Fock CI, see(a) Takeda, R.; Yamanaka, S.; Yamaguchi, K. *Int. J. Quantum Chem.* **2006**, *106*, 3303. (b) Takeda, R.; Yamanaka, S.; Yamaguchi, K. *Int. J. Quantum Chem.* **2007**, *107*, 3219. (c) Nishihara, S.; Yamanaka, S.; Ukai, T.; Nakata, K.; Kusakabe, K.; Yonezawa, Y.; Nakamura, H.; Takada, T.; Yamaguchi, K. *Int. J. Quantum Chem.* **2008**, *108*, 2966. For the resonating coupled-cluster CI, see (d) Yamanaka, S.; Nishihara, S.; Nakata, K.; Yonezawa, Y.; Okumura, M.; Takada, T.; Nakamura, H.; Yamaguchi, K. *Int. J. Quantum Chem.* **2009**, *109*, 3811.

(28) (a) Vanderslice, J. T.; Mason, E. A.; Maisch, W. G. *J. Chem. Phys.* **1960**, *32*, 515. (b) *Kagaku Binran (Handbook of Chemistry)*, 5th ed.; The Chemical Society of Japan: Tokyo, 2004.

(29) Isobe, H.; Yamanaka, S.; Kuramitsu, S; Yamaguchi, K. *J. Am. Chem. Soc.* **2008**, *130*, 132.

(30) (a) Groves, J. T.; McClusky, G. A. *J. Am. Chem. Soc.* **1976**, *98*, 859. (b) Groves, J. T.; McGlusky, G. A.; White, R. E.; Coon, M. J. *Biochem. Biophys. Res. Commun.* **1978**, *81*, 154. (c) Groves, J. T. *J. Chem. Educ.* **1985**, *62*, 928. (d) Auclair, K.; Hu, Z.; Little, D. M.; Ortiz de Montellano, P. R.; Groves, J. T. *J. Am. Chem. Soc.* **2002**, *124*, 6020.

(31) Altun, A.; Shaik, S.; Thiel, W. *J. Am. Chem. Soc.* **2007**, *129*, 8978.

(32) Sawyer, D. T. *Oxygen Chemistry*; Oxford University Press: NewYork, 1991.

(33) The potential curves of the ^{4}**1**, ^{2}**1**, ^{2}**1**′, ^{2}**1**″, ^{2}**1***, and ^{4}**1*** configurations as a function of r_{FeO} are presented in Figure S3. Although ^{4}**1*** could be located close in energy to ^{2}**1*** in the region of sufficiently long Fe−O bond distances (r_{FeO} > 1.96 Å), calculations at any distance of r_{FeO} < 1.96 Å always converged to the lower-lying ferryl−oxo configuration ^{4}**1**, which indicates that ^{4}**1*** is unstable.